

Characterization of New Pentanuclear Copper(II) and REE(III) Carboxylate Complexes

O. S. Pushikhina^{a, *}, E. V. Karpova^{a, **}, D. A. Tsarev^b, V. A. Tafeenko^a, and T. B. Shatalova^a

^a Moscow State University, Moscow, 119991 Russia

^b Mitoengineering Research Institute, Moscow State University, Moscow, 119991 Russia

*e-mail: pushikhina_chem@mail.ru

**e-mail: karpova@inorg.chem.msu.ru

Received April 28, 2023; revised June 13, 2023; accepted June 14, 2023

Abstract—New pentanuclear complexes $[\text{Cu}_3\text{M}_2(\text{CHF}_2\text{COO})_{12}(\text{H}_2\text{O})_8]\cdot 2\text{H}_2\text{O}$, where M = Er (**I**) and Nd (**II**), were synthesized by reacting individual copper haloacetates and REE in aqueous solution. The molecular structure of complex **I** was determined by single crystal X-ray diffraction analysis (CIF file CCDC no. 2159724). The structural features of the complexes and the nature of the carboxylate bridges between the metal centers affect the properties of these complexes; therefore, two similar compounds with the monochloroacetate ligand were prepared for comparison: $[\text{Cu}_3\text{M}_2(\text{CH}_2\text{ClCOO})_{12}(\text{H}_2\text{O})_8]\cdot 2\text{H}_2\text{O}$, where M = Er (**III**) and Nd (**IV**). Compounds **III** and **IV** are isostructural to previously studied complexes of this type with other REE. Compounds **I–IV** were characterized by X-ray diffraction analysis and IR spectroscopy, and their thermal behavior was studied. To confirm the formation of precursors of molecular species of crystalline compound **I**, the solute species of the complexes were determined by electrospray ionization mass spectrometry (ESI-MS).

Keywords: heterometallic complex, complex species, haloacetate, crystal structure, thermal analysis

DOI: 10.1134/S0036023623601678

INTRODUCTION

Polynuclear heterometallic complexes are of particular interest in the context of elucidating the nature of exchange interactions between ions of transition metals and rare-earth elements (REE) linked to one another by bridging ligands [1–3]. Exchange interactions can be accomplished not only through the shortest metal–element (E)–metal channels, but also through conjugated M–O–E–O–M bonds: through nitrate, carbonate, phosphate, or vanadate ions, as well as through triflate and carboxylate ions [4]. The nature of the exchange depends on the types of orbitals of the metal atom, on the number of electrons on them, and on the location of the intermediary atoms [5]. Now, a large number of metal carboxylates have been prepared that exhibit magnetic properties; two main types of crystal structures can be distinguished among them: molecular structures and extended structures [6–8]. It is of great scientific importance to develop synthetic approaches for the preparation of heterometallic complexes with low spin system dimensions based on $3d$ – $4f$ metals and carboxylate ligands.

In this work, we prepared and studied new pentanuclear heterometallic complexes $[\text{Cu}_3\text{M}_2(\text{CHF}_2\text{COO})_{12}(\text{H}_2\text{O})_8]\cdot 2\text{H}_2\text{O}$, where M = Er (**I**) and Nd (**II**). Carboxylates with a similar metal core Cu_3M_2 were previously studied in a number of works,

where monochloroacetate complexes with Gd [9], Pr, Nd, Sm, Dy, Ho [10], Yb [11], and Y [12] were prepared by reacting copper and REE nitrates with monochloroacetic acid. The erbium compound (**III**) and neodymium compound (**IV**) were prepared to compare properties. Although the structure of compound **IV** was determined [10], there are no relevant spectral data and no information on the thermal stability of this compound.

Haloacetates can participate as ligands in the formation of various types of polynuclear heterometallic structures. One can be aware from the related literature [13] that the compound $\text{CuNd}_2(\text{CCl}_3\text{COO})_8(\text{H}_2\text{O})_6$ can be formed, which structure is built of chain moieties where a monomer unit contains two neodymium ions and one copper ion. We found that, in the case of monochloroacetic and difluoroacetic acids, pentanuclear complexes **I–IV** with the metal ratio 3 : 2, which are likely to be more stable, are formed in the solutions with the initial ratio Cu : REE = 1 : 2 under synthesis conditions similar to those used in [13].

Understanding of the processes involved in the formation of precursors of a crystalline form of the compound in solution is a key aspect in the practicability of a targeted design of coordination compounds with custom compositions and structures. Electrospray

ionization mass spectrometry (ESI-MS) is a tool to identify the compositions of all complex species in the solution. In addition, this method allows to study not only individual complexes, but also the formation dynamics and changes in the speciation of these complexes under various conditions.

Here, we will discuss the properties of four heterometallic haloacetate compounds of copper and REE and compare these data to those in the related literature.

EXPERIMENTAL

Compounds **I–IV** were prepared by solution chemistry methods. The first stage in the synthesis of heterometallic haloacetates was to prepare individual (homometallic) copper, neodymium, and erbium compounds. The commercially available chemicals used as-received for this purpose were: basic copper carbonate $(\text{CuOH})_2\text{CO}_3$, neodymium oxide Nd_2O_3 , erbium oxide Er_2O_3 , acids CH_2ClCOOH , and CHF_2COOH of chemically pure grade. Individual metal salts $\text{Cu}(\text{CH}_2\text{ClCOO})_2(\text{H}_2\text{O})_{1.5}$, $\text{Cu}(\text{CHF}_2\text{COO})_2(\text{H}_2\text{O})_{0.5}$, $\text{M}(\text{CH}_2\text{ClCOO})_3(\text{H}_2\text{O})_{5/3}$, and $\text{M}(\text{CHF}_2\text{COO})_3(\text{H}_2\text{O})_3$, where $\text{M} = \text{Er}$ and Nd , were prepared based on known procedures [14–16].

*Synthesis of $[\text{Cu}_3\text{M}_2(\text{CHF}_2\text{COO})_{12}(\text{H}_2\text{O})_8] \cdot 2\text{H}_2\text{O}$, where $\text{M} = \text{Er}$ (**I**) and Nd (**II**)*

A mixture of 1.5 mmol $\text{Cu}(\text{CHF}_2\text{COO})_2(\text{H}_2\text{O})_{0.5}$ and 1 mmol $\text{Er}(\text{CHF}_2\text{COO})_3(\text{H}_2\text{O})_3$ was dissolved in 5 mL water. The solution was concentrated in an ajar vial at room temperature. As a result, air stable intense blue crystals formed in the solution. The composition and structure of compound **I** were determined by single-crystal X-ray diffraction. Compound **II** was prepared by a similar procedure from copper and neodymium salts. The prepared compounds were isostructural.

IR spectrum (ν , cm^{-1}) for **I**: 3403 w $\nu(\text{OH})$, 1707 m, 1657 s, 1612 s $\nu_{\text{as}}(\text{COO})$, 1471 m $\nu_{\text{s}}(\text{COO})$, 1331 s $\delta(\text{CH})$, 1112 s, 1060 s $\nu(\text{CF}_2)$, 954 m $\delta(\text{CCF})$, 813 m $\nu(\text{CC})$.

IR spectrum (ν , cm^{-1}) for **II**: 3402 w $\nu(\text{OH})$, 1703 m, 1656 s, 1610 s $\nu_{\text{as}}(\text{COO})$, 1468 m $\nu_{\text{s}}(\text{COO})$, 1330 s $\delta(\text{CH})$, 1117 s, 1059 s $\nu(\text{CF}_2)$, 954 m $\delta(\text{CCF})$, 813 m $\nu(\text{CC})$.

*Synthesis of $[\text{Cu}_3\text{M}_2(\text{CH}_2\text{ClCOO})_{12}(\text{H}_2\text{O})_8] \cdot 2\text{H}_2\text{O}$, Where $\text{M} = \text{Er}$ (**III**) and Nd (**IV**)*

Compounds (**III**) and (**IV**) were prepared, like compound **I** was, by reacting the individual metal monochloroacetates, with the only difference that here crystallization was kinetically hindered because of a higher viscosity of the saturated solution. Newly prepared compound **III** is isostructural to the previ-

ously characterized Gd, Pr, Nd, Sm, Dy, Ho, Yb, and Y complexes [9–12]. The procedure used can yield known compound **IV**, whose structure was determined by Voronkova et al. [10]. It should be mentioned that it is undesirable to concentrate solutions containing monochloroacetate ions under heating for they decompose to release chloride ions, while difluoroacetates are more resistant to heating.

IR spectrum (ν , cm^{-1}) for **III**: 3602 w, 3342 m $\nu(\text{OH})$, 3013 w, 2958 w $\nu(\text{CH}_2)$, 1670 m, 1602 s, 1563 s $\nu_{\text{as}}(\text{COO})$, 1396 s $\nu_{\text{s}}(\text{COO})$, 1253 m, 970 w $\delta(\text{CH}_2)$, 931 m $\nu(\text{CC})$, 711 m $\nu(\text{CCl})$, 790 m, 696 m $\delta(\text{COO})$.

IR spectrum (ν , cm^{-1}) for **IV**: 3590 w, 3353 m $\nu(\text{OH})$, 3013 w, 2958 w $\nu(\text{CH}_2)$, 1665 m, 1607 s, 1561 s $\nu_{\text{as}}(\text{COO})$, 1399 s $\nu_{\text{s}}(\text{COO})$, 1255 m, 967 w $\delta(\text{CH}_2)$, 933 m $\nu(\text{CC})$, 710 m $\nu(\text{CCl})$, 793 m, 675 m $\delta(\text{COO})$.

Single-Crystal X-ray Diffraction (XRD)

Structure data were deposited with the Cambridge Center for Crystallographic Data (No. 2159724 (**I**); deposit@ccdc.cam.ac.uk; www: http://www.ccdc.cam.ac.uk). The crystal data and refinement details are given in Table 1. Characteristic interatomic distances and bond angles appear in Table 2. The data were collected on a StadiVari STOE diffractometer with a Pilatus100K 2D detector using CuK_α radiation ($\lambda = 1.54186 \text{ \AA}$). The structure was solved by direct methods and refined by least squares for F^2 with the SHELX software [17–19]. The positional and thermal parameters of non-hydrogen atoms were refined in the full-matrix anisotropic approximation. The hydrogen atoms were positioned using a riding model. Structure images were prepared in the DIAMOND program [20].

X-ray Powder Diffraction (PXRD)

X-ray powder diffraction patterns of polycrystalline samples of compounds **I–IV** were recorded on a Rigaku D/MAX 2500 diffractometer with a rotating anode in the reflection mode using CuK_α radiation and a graphite monochromator and on a STOE STADI IP diffractometer in the transmission mode (CuK_α radiation, Ge(111) monochromator).

Thermal Analysis

The thermal behavior of samples **I–IV** was studied by a Netzsch STA 409PC Luxx® simultaneous thermal analyzer interfaced with a Netzsch QMS 403 C Aëolos® quadrupole mass spectrometer. Samples (ca. 10 mg) were heated to 800°C at 2°C/min in a dynamic argon flow (30 mL/min) in an alundum crucible. The mass spectra of decomposition products were recorded over the entire temperature range under investigation. The thermoanalytical curves and mass spectra were processed in Netzsch Proteus® software.

IR Spectroscopy

The IR absorption spectra of crystalline samples of compounds **I–IV** were recorded on a Nicolet 8700 Thermo Scientific (attenuated total reflectance (ATR) mode, 4 cm⁻¹ resolution) and Perkin-Elmer Spectrum 3 (ATR mode, 2 cm⁻¹ resolution) in the range 4000–650 cm⁻¹.

ESI Mass Spectrometry

The formation of precursors of molecular species of compound **I** in aqueous solution (1 mg/mL) was studied by ESI-MS in positive (+ESI) and negative (-ESI) ion detection modes on a Waters ACQUITY TQD tandem mass-spectrometric detector in the range of mass numbers (*m/z*) from 50 to 2000.

RESULTS AND DISCUSSION

A series of syntheses with different ratios of metal salts was carried out to prepare heterometallic compounds with extended structural moieties.

Compounds **I–IV** were formed when there was a clear excess of one of the metals in the reaction mixture, for example, when the copper-to-REE metal ion molar ratio was 1 to 2, which indicates the high stability of this pentanuclear molecular moiety. Crystallization in such solutions is kinetically hindered, and a multicomponent solid phase is formed upon crystallization (Fig. S1). When the proportion of REE salts in the syntheses increased, the crystallinity of the products decreased and amorphous precipitates were formed.

We optimized the synthetic procedure to provide an amount of a single-phase product sufficient for it to be characterized by PXRD, TG, ESI-MS, and IR spectroscopy.

As shown by XRD (Tables 1 and 2), complex **I** is built of centrosymmetric chain pentanuclear molecular moieties with a linear sequence of metal ions Cu(1)–Er(1)–Cu(2)–Er(1)–Cu(1) linked by bridging carboxylate groups (Fig. 1).

Compounds **I–IV** have the same coordination framework formula, but despite their very similar crystallographic characteristics (Table 3), they are not isostructural. Hereafter in the text, such compounds will be referred to as *isotypical*. The atomic sizes and inductive effect of the substituent at the carboxyl group are comparable and lead to the formation of compounds with similar structures. It should be mentioned that such trifluoro- and trichloroacetate complexes could not be synthesized for a number of reasons: the acid strength, structures of individual copper and REE salts, and steric factors.

The substituent effect increases in the CH₃COOH, CH₂ClCOOH, CHF₂COOH, CCl₃COOH, and CF₃COOH series; the electron-donating ability of the oxygen atom weakens, and this affects the characteristics of the bonds formed. The higher ionicity of the metal–oxygen bond for the trifluoroacetate ion can

Table 1. Selected crystallographic characteristics and details of the single-crystal X-ray diffraction experiment for compound **I**

| Parameter | Value |
|---|---|
| Formula unit | C ₁₂ H ₁₆ Cu _{1.5} ErF ₁₂ O ₁₇ |
| Formula weight | 922.82 |
| Crystal system | Monoclinic |
| Space group | <i>P</i> ₂ ₁ / <i>c</i> |
| <i>a</i> , Å | 10.2339(5) |
| <i>b</i> , Å | 17.2025(8) |
| <i>c</i> , Å | 15.6227(8) |
| α , deg | 90 |
| β , deg | 97.281(4) |
| γ , deg | 90 |
| <i>V</i> , Å ³ | 2728.2(2) |
| <i>Z</i> | 4 |
| <i>T</i> , K | 295(2) |
| $\rho_{\text{calcd.}}$, g/cm ³ | 2.247 |
| μ , mm ⁻¹ | 8.378 |
| <i>F</i> (000) | 1774 |
| Crystal size, mm | 0.12 × 0.14 × 0.23 |
| θ scan range, deg | 3.839–70.685 |
| <i>hkl</i> ranges | –12 ≤ <i>h</i> ≤ 7 –21 ≤ <i>k</i> ≤ 20 –19 ≤ <i>l</i> ≤ 15 |
| Measured/unique reflections | 19580/5125 |
| <i>R</i> _{int} | 0.0725 |
| Reflections with <i>I</i> > 2 σ (<i>I</i>) | 4295 |
| GOOF | 1.058 |
| <i>R</i> -factors (<i>I</i> > 2 σ (<i>I</i>)) | <i>R</i> ₁ = 0.0629 <i>wR</i> ₂ = 0.1776 |
| <i>R</i> -factors (over all reflections) | <i>R</i> ₁ = 0.0708 <i>wR</i> ₂ = 0.1838 |
| Residual electron density (min/max), e/Å ³ | –1.344/1.829 |

render the formation of heterometallic compounds unfavorable, and ultimately can lead to the formation of individual compounds. Differences between the structures of individual copper salts can also be the reason for the formation of individual rather than heterometallic compounds. Copper trichloroacetate [15] and copper trifluoroacetate [16] crystal hydrates have a molecular crystal structure motif formed by mononuclear species. Copper monochloroacetate [15] and copper acetate [21] crystal hydrates have paddle wheel structures: binuclear discrete moieties in which copper ions are linked in pairs by four bridging RCOO⁻ ligands. Copper acetate has the highest stability of this

Table 2. Comparison of characteristic interatomic distances and bond angles in the series of isotypical compounds: prepared compound **I** and known $[\text{Cu}_3\text{M}_2(\text{CH}_2\text{ClCOO})_{12}(\text{H}_2\text{O})_8]\cdot 2\text{H}_2\text{O}$ compounds, where M = Nd [10], Gd [9], Dy [10], and Yb [11]. The values refer to a metal atom–carboxylate oxygen atom pair

| Compound | [Cu(2)] planar square | | | [Cu(1)] paddle wheel | | | | |
|----------|------------------------|----------|-----------|-------------------------|------------------------|-----------|--------------------------|-----------------------|
| | Cu–O, Å | M–O, Å | Cu–M, Å | Cu–O, Å | M–O, Å | Cu–M, Å | O–Cu–O, deg | O–M–O, deg |
| I | 1.957(5) 1.955(5) | 2.282(5) | 3.5588(1) | 1.943(6)– 1.986(5) | 2.295(6)– 2.330(5) | 4.6472(2) | 171.7(2)– 172.4(2) | 116.3(2)– 117.4(2) |
| M = Nd | 1.954(3) 1.964(3) | 2.385(3) | 3.601(2) | 1.965(3)– 1.990(3) | 2.366(3)– 2.452(4) | 4.654(2) | 173.20(13)– 175.51(3) | 113.6(1)– 116.7(1) |
| M = Gd | 1.959(4) 1.970(5) | 2.337(4) | 3.561(1) | 1.956(4)– 1.979(4) | 2.325(3)– 2.397(5) | 4.662(1) | 172.4(2)– 174.4(2) | 114.4(2)– 117.9(2) |
| M = Dy | 1.950(3) 1.950(3) | 2.299(3) | 3.535(1) | 1.954(3)– 1.987(3) | 2.298(4)– 2.369(3) | 4.621(1) | 173.2(1)– 174.5(1) | 116.4(1)– 118.5(1) |
| M = Yb | 1.936(11) 1.952(10) | 2.269(9) | 3.506(2) | 1.959(11)– 1.985(12) | 2.274(9)– 2.351(11) | 4.620(1) | 172.0(4)– 173.4(5) | 116.8(4)– 118.8(4) |

moiety, so the formation of heterometallic compounds is not observed for acetic acid. Copper difluoroacetate is known for its layered 2D polymer structure [16]. The copper coordination polyhedron in all of the listed compounds is a square pyramid, except

for copper trifluoroacetate hydrate: its polyhedron is a tetragonally distorted octahedron.

The crystal structure of REE trifluoroacetates is built of binuclear moieties [22, 23], which, in turn, promotes the primary crystallization of these com-

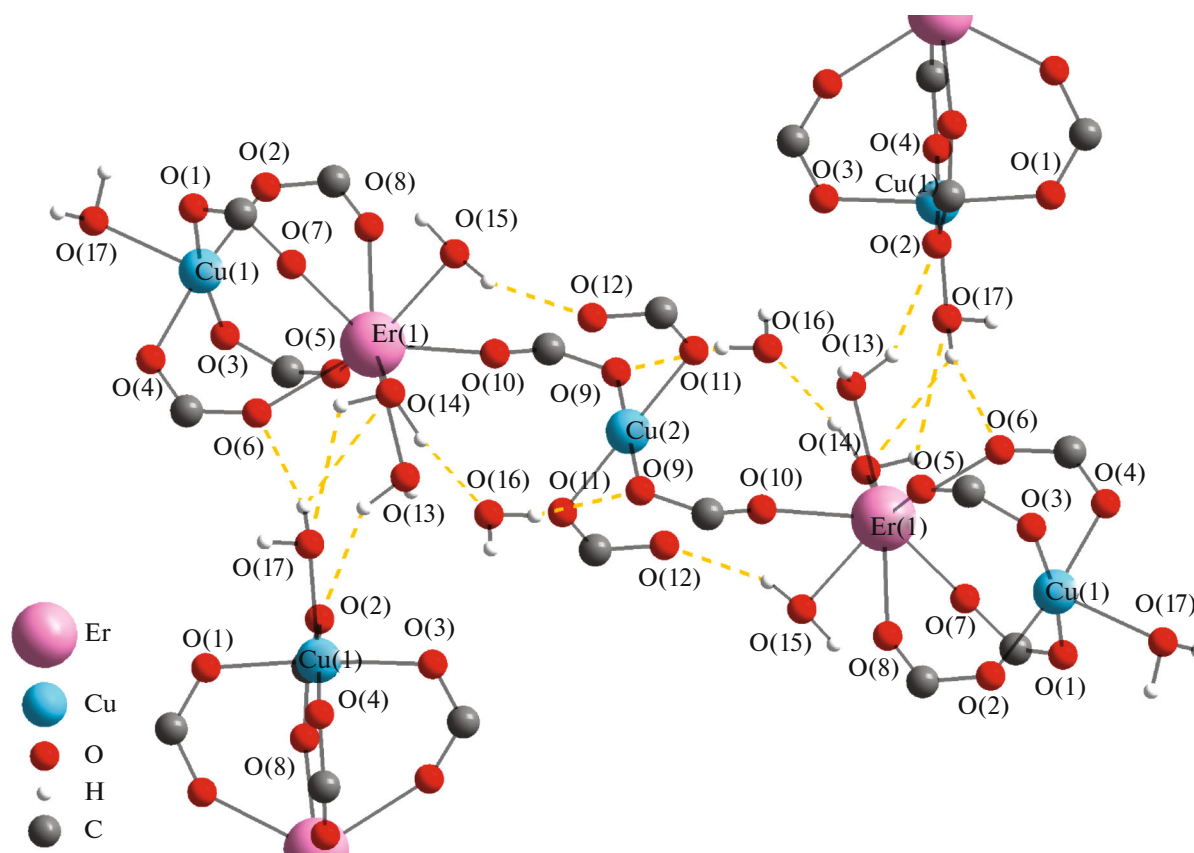


Fig. 1. Molecular moiety of the structure of compound **I** and its binding via hydrogen bonds (dashed lines) with neighboring moieties. The difluoromethyl groups are hidden.

Table 3. Comparison of unit cell parameters in the series of newly prepared and known isotypical compounds (space group $P2_1/c$)

| Parameter | [Cu ₃ M ₂ CHF ₂ COO] ₁₂ (H ₂ O) ₈ ·2H ₂ O | | [Cu ₃ M ₂ (CH ₂ ClCOO) ₁₂ (H ₂ O) ₈ ·2H ₂ O | | | |
|--------------|--|------------|--|-----------|-----------|-----------|
| | Nd* | Er** | Nd [10] | Gd [9] | Dy [10] | Yb [11] |
| <i>a</i> , Å | 10.2464 (6) | 10.2339(5) | 10.4980(2) | 10.521(2) | 10.408(2) | 10.424(6) |
| <i>b</i> , Å | 17.5934(11) | 17.2025(8) | 17.9960(3) | 18.024(4) | 17.838(4) | 17.953(4) |
| <i>c</i> , Å | 15.7001(8) | 15.6227(8) | 15.0760(4) | 15.310(3) | 15.010(3) | 15.193(4) |
| β, deg | 98.098(4) | 97.281(4) | 99.3500(6) | 99.85(3) | 99.65(3) | 100.18(1) |

* The result of indexing of the powder pattern of a sample of compound **II** (Fig. S2).

** Single-crystal X-ray diffraction data for compound **I**.

pounds. Rare-earth trichloroacetates, monochloroacetates, and difluoroacetates, however, are 1D polymers [24–26]. The coordinative capabilities of REE atoms are determined by their sizes: bridging anions are evenly distributed along the chain, and water molecules supplement the environment of metal centers to the largest possible (CN = 8–9).

The coordinative capabilities of copper and REE atoms open up a huge variability of extended (polymeric) heterometallic structures; in our case, however, it is more appropriate to talk about oligomerization: a pair of CuML₄ building blocks combined with another copper atom organizes a stable pentanuclear unit that cannot polymerize further. One possible reason for the formation of an oligomeric structure instead of a polymeric one can be the centrosymmetric square-planar CuL₄ moiety with the Cu(2) atom, which turned out to be a framework-forming element in this structure. This complex species is unique in that the metal ions therein are linked exclusively by bridging carboxyl groups, and the molecule itself is not stabilized by other polydentate ligands, such as Schiff bases [27–29].

When packed in a crystal, pentanuclear molecular moieties and cavity water molecules are linked by hydrogen bonds to form a three-dimensional structure (Fig. 2). A large number of short contacts and a dense cross-arrangement of molecular moieties lead to the fact that the characteristic distances between metal atoms and oxygen atoms of water molecules do not increase (Er–O 2.326–2.401(5) Å and Cu–O 2.190(6) Å), as described [24]. All the ten water molecules in the structure of **I** are involved in binding (O–H···O 2.798–3.591(9) Å), where most oxygen atoms perform as both hydrogen-bond acceptors and donors, each forming two or three such contacts.

Single-crystal X-ray diffraction data match the X-ray powder diffraction experiment ($R_{\text{obs}} = 5.18\%$, $wR_{\text{obs}} = 6.31\%$, $R_{\text{all}} = 5.18\%$, $wR_{\text{all}} = 6.31\%$, $\text{GOOF} = 3.23$, $R_p = 9.67\%$, $wR_p = 12.70\%$), verifying the phase purity of the sample (Fig. S3).

Formation of Precursors of Molecular Complex Species in Solution

Electrospray ionization mass spectrometry can help to study the formation of precursors of molecular complex species in solution. Electrospray is a very mild ionization method, so the mass spectra of com-

pounds prepared by this ionization method usually do not feature peaks of fragmentation ions [30]. It is pertinent to mention here that, when the choice of experimental conditions is unsuccessful or when thermolabile compounds are analyzed, the mass spectra may feature peaks corresponding to both fragmentation and adduct ions.

The intensity of adduct ions and the number of adducts strongly depend on the experimental conditions. As a rule, the intensities of molecular and pseudo-molecular ions increase as the cone voltage increases, while the total intensity of adduct ions decreases (in this case, the relative intensities of adduct ions change to increase the intensities of those ions that contain smaller numbers of attached solvent molecules). For a methanolic solution of CuCl₂, it was shown that the [Cu(MeOH)₂]⁺ and [Cu(MeOH)]⁺ adduct ions had their intensities decreased significantly when the cone voltage increased from 40 to 60 V, with an attendant increase in [Cu]⁺ ion intensity [31].

Our ESI-MS experiment in the –ESI mode at the optimal voltage detected the ions listed in Table 4.

The ion isotope clusters match the calculations (MassLynx, Isotope Model tool). An example is the

Table 4. Referring the *m/z* values to suggested ion/adduct compositions. The values refer to the ion of the highest intensity in the isotopic cluster; the values are rounded to an integer

| <i>m/z</i> | Suggested composition |
|------------|---|
| 95 | [CHF ₂ COO] [–] |
| 113 | [CHF ₂ COO [–] + H ₂ O] [–] |
| 253 | [Cu ⁺ (CHF ₂ COO [–]) ₂] [–] |
| 348 | [Cu ⁺² (CHF ₂ COO [–]) ₃] [–] |
| 366 | [Cu ⁺² (CHF ₂ COO [–]) ₃ + H ₂ O] [–] |
| 546 | [Er ⁺³ (CHF ₂ COO [–]) ₄] [–] |
| 801 | [Er ⁺³ Cu ⁺² (CHF ₂ COO [–]) ₆] [–] |
| 819 | [Er ⁺³ Cu ⁺² (CHF ₂ COO [–]) ₆ + H ₂ O] [–] |
| 1054 | [Er ⁺³ Cu ⁺² (CHF ₂ COO [–]) ₈] [–] |
| 1072 | [Er ⁺³ Cu ⁺² (CHF ₂ COO [–]) ₈ + H ₂ O] [–] |
| 1506 | [Er ₂ ⁺³ Cu ⁺² (CHF ₂ COO [–]) ₁₁] [–] |

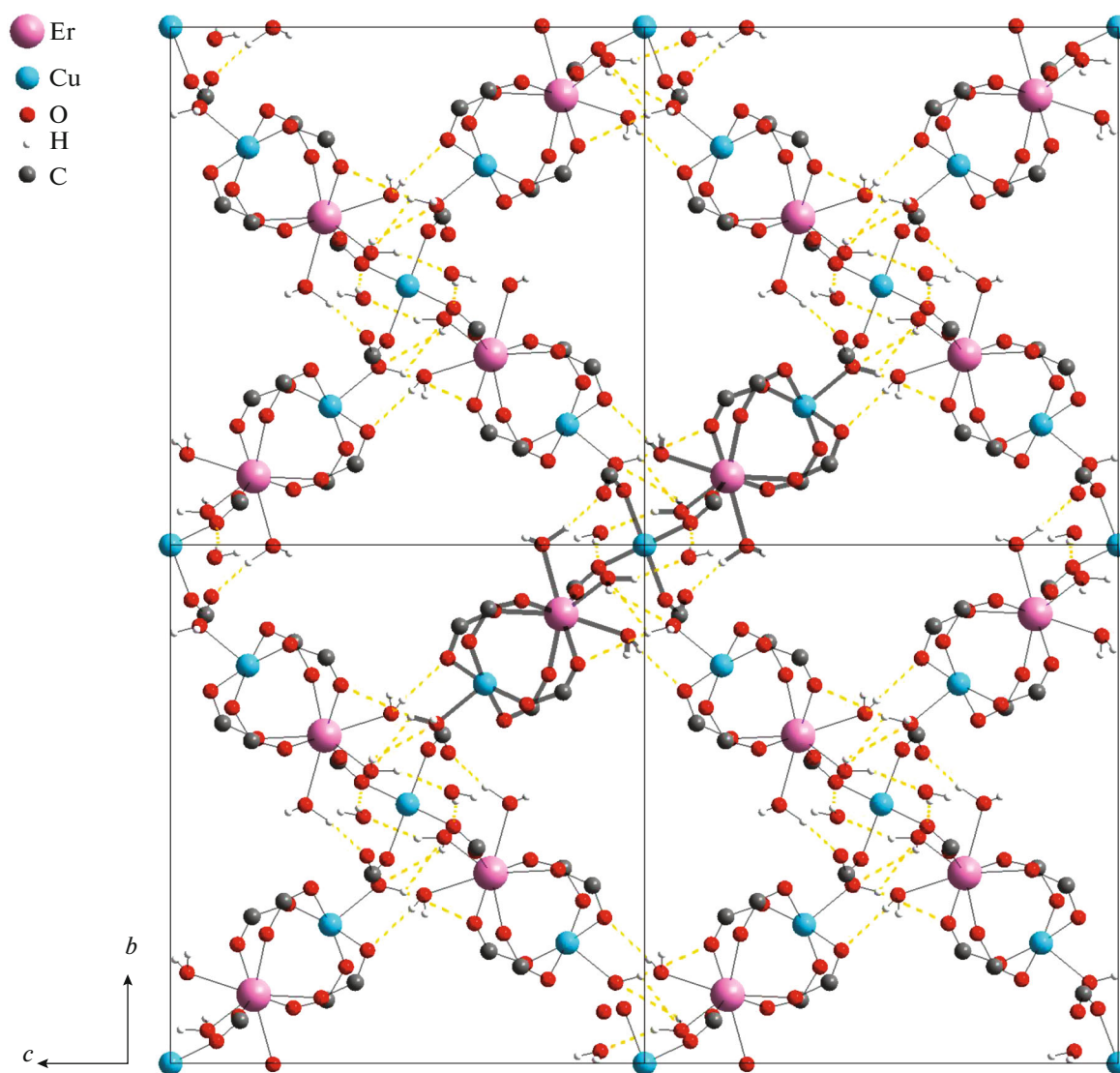


Fig. 2. Arrangement of moieties in the crystal structure of compound **I** in plane *bc*. The hydrogen bonds are shown. The difluoromethyl groups are hidden for clarity.

calculated and experimentally observed isotope clusters for the $m/z = 1054$ ion (Fig. 3).

The appearance of the $m/z = 253$ ion containing copper(I) may be explained by the redox reaction in the ionization chamber of the mass spectrometer. At present, the possibility of redox reactions to occur during electrospray ionization has been shown for ions of various metals (Cu, Hg, and Fe), and this is a well-known fact [32].

Figure 4 shows the complete mass spectrum of negatively charged ions in the range of m/z values from 50 to 2000. Comparing the observed isotope clusters with calculated isotope patterns, we may infer that the $m/z < 400$ ions do not contain erbium, i.e., are not target ions.

The appearance of ions with m/z values equal to 801, 1054, and 1506 in the mass spectrum of the sample may serve as evidence for the possible formation in solution of relatively stable ionic associates with alternating copper and erbium atoms linked by carboxyl groups of difluoroacetic acid ions. These associates are precursors of the molecular species of complex **I**. Their occurrence in solution serves as a confirmation of the suggestion about oligomerization.

An inspection of the +ESI mass spectra showed the presence of peaks corresponding to copper-containing ions and the absence of peaks corresponding to erbium-containing ions.

IR spectroscopy is a tool to determine coordination modes. Carboxylate groups can be coordinated by

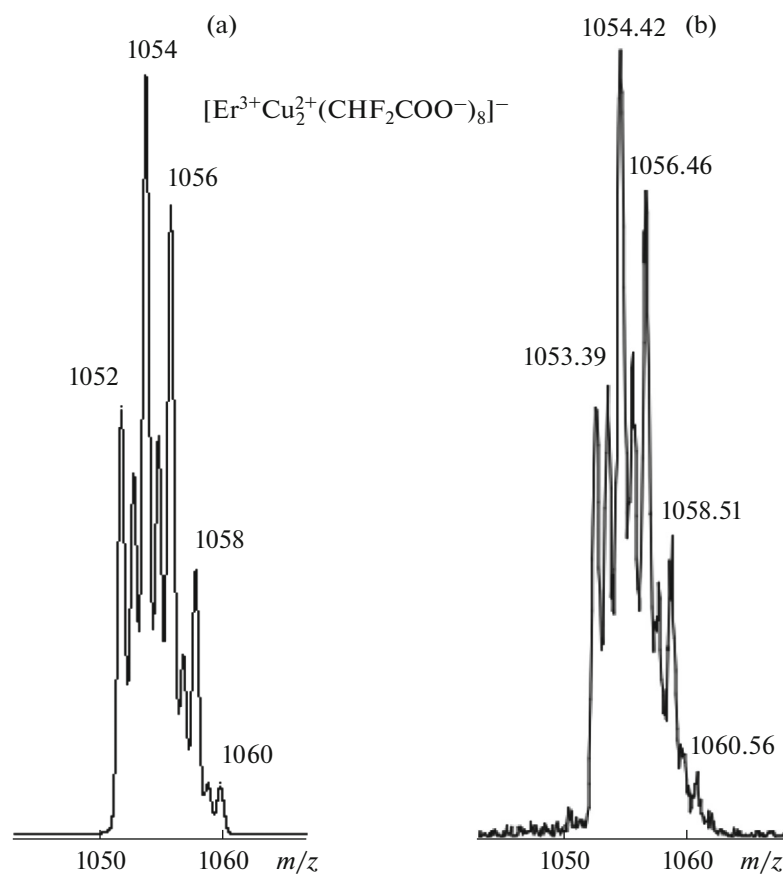


Fig. 3. (a) Calculated and (b) observed isotopic clusters for the $m/z = 1054$ ion.

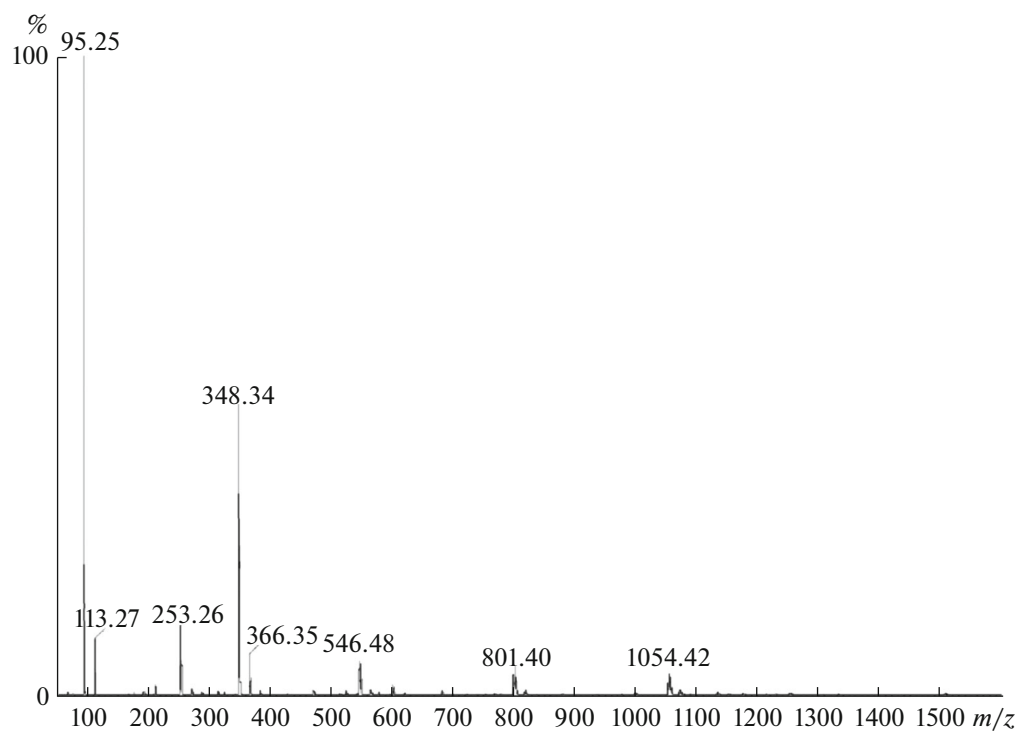


Fig. 4. Mass spectrum of a sample of compound I.

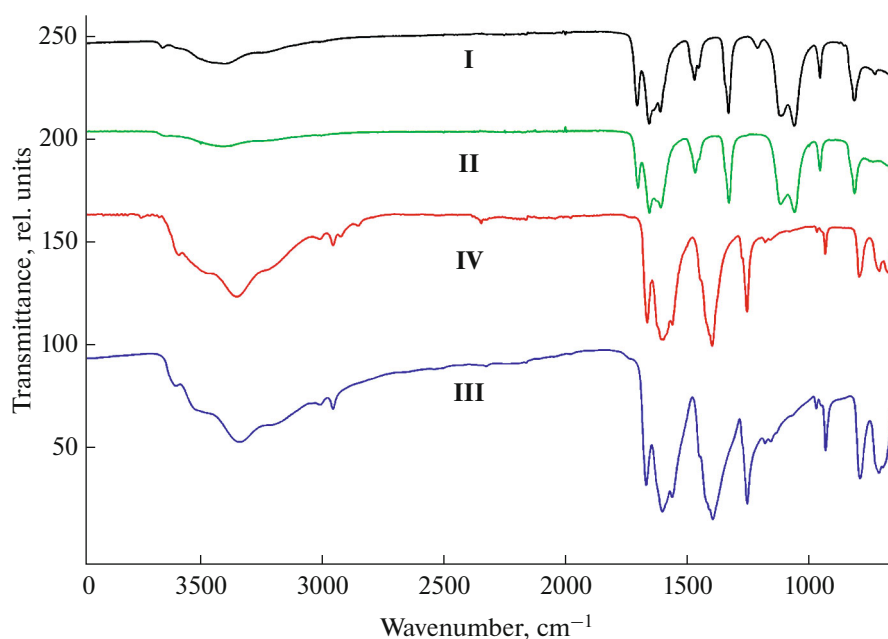


Fig. 5. ATR-IR spectra of crystalline samples of compounds I–IV.

metal ions in various ways. It is known that, if the difference (Δ) between the frequencies of asymmetric and symmetric stretching O–C–O vibrations is less than in the free carboxylate ion, this is considered an indicator of bridging-bidentate binding or of a chelating carboxyl group; and if Δ is greater, then this indicates the monodenticity (pseudo-ether coordination) of the ligand [33]. This trend can be traced in the analysis of the transmission spectra of the prepared pentanuclear complexes, in which carboxyl ligands have different functions. Three groups of equivalent ligands differing in bond lengths and O–C–O angles can be distinguished in the structure: pseudo-ether (monodentate) ligands, bridging ligands in paddle wheel moieties, and bridging ligands to the central copper ion. Figure 5 shows our measured ATR-IR spectra of crystalline samples of compounds I–IV.

The IR spectra of difluoroacetate complexes **I** and **II** follow each other's contours as expected. The characteristic strong bands of the asymmetric ($\nu_{\text{as}}(\text{COO})$) and symmetric ($\nu_{\text{s}}(\text{COO})$) stretching vibrations appear at 1707–1610 and 1470 cm^{-1} , respectively. The resolution of the $\nu_{\text{as}}(\text{COO})$ band set may be explained in terms of the above-described structural function of the ligand. In the spectrum of a free difluoroacetate ion (NaCHF_2COO), Δ is ca. 200 cm^{-1} [34]. The $\nu_{\text{as}}(\text{COO})$ band is split to three peaks; for the left, more distant peak, $\Delta = 236 \text{ cm}^{-1}$, indicating its belonging to the $\nu_{\text{as}}(\text{COO})$ mode of monodentate ligands, and the central and the right-hand peaks with the Δ equal to 186 and 141 cm^{-1} , respectively, belong to the $\nu_{\text{as}}(\text{COO})$ modes of bridging ligands.

The substituent effect on the stretching frequencies of the carboxyl group increases in the series $\text{CH}_2\text{Cl} < \text{CHF}_2$ due to the greater inductive effect of the fluoro substituent. In the spectra of monochloroacetate complexes **III** and **IV**, the O–C–O stretching vibration bands shift toward the longer wavelengths: $\nu_{\text{as}}(\text{COO})$ appears at 1670–1561 cm^{-1} , and $\nu_{\text{s}}(\text{COO})$ appears at 1398 cm^{-1} . Keeping in mind that compounds I–IV under consideration are isotypical, we can conclude that the bands assigned to bond vibrations in ligands with different structural functions shift synchronously and have similar assignments; the Δ calculations confirm this conclusion.

It is due to the same effect that the band related to the skeletal vibrational mode ν_{CC} , which appears at 813 cm^{-1} in the spectra of compounds **I** and **II**, shifts from its position at 932 cm^{-1} in **III** and **IV**. The C–C bond is irresponsive to the coordination mode of the carboxylate ligand, so the band is not split.

The C–H bending vibrations in monochloromethyl and difluoromethyl groups appear in the spectra as strong bands at 1254 cm^{-1} for **III** and **IV**, assigned to the $\delta(\text{CH}_2)$ mode in monochloroacetate, and at 1331 cm^{-1} for **I** and **II**, assigned to the δCH mode in difluoroacetate.

Two strong bands in the spectra of **I** and **II** that appear in the range from 1117 to 1059 cm^{-1} relate to the stretching vibrations $\nu(\text{CF}_2)$. The medium-intensity band at 711 cm^{-1} in the spectra of **III** and **IV** relates to the stretching vibrations νCCl , and the set of low-intensity bands in the range from 3020 to 2950 cm^{-1} is due to the stretching vibrations $\nu(\text{CH}_2)$. Absorption in the

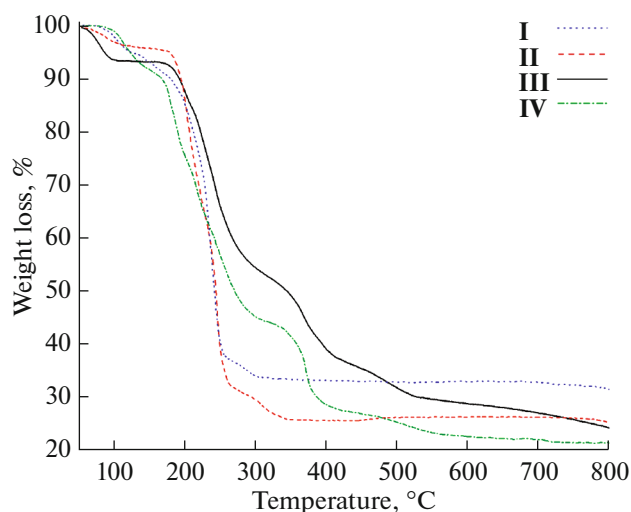


Fig. 6. TG curves for samples of compounds I–IV.

short-wavelength range in all spectra at $3700\text{--}3100\text{ cm}^{-1}$ corresponds to the stretching vibrations $\nu(\text{OH})$ of water molecules involved in hydrogen bonding, and this correlates with XRD data.

Thermal Behavior

Analysis of the thermal behavior of compounds I–IV distinguishes two general stages of decomposition (dehydration and decarboxylation) where the major weight loss occurs; then, depending on the ligand, the curves diverse significantly (Fig. 6).

Let us consider the first thermal destruction stage for compounds I and II. Dehydration proceeds over a wide temperature range, as evidenced by an increase in intensities on H_2O^+ ion current curve ($m/z = 18$) (Fig. 7). A weight loss of about 10% up to 180°C according to the DTG curve and ion current mass spectra corresponds to removal of both interstitial hydrogen-bonded water molecules and water molecules coordinated to metal centers. The release of water molecules is accompanied by the appearance of OH^+ fragmentation ions, due to which hydroxo complexes can be among the intermediate products.

The second degradation stage involves significant weight loss of about 55% up to 270°C . Ion currents with the same m/z values are detected in this range, but here they relate to the fragmentation products of haloacetate groups. The ion current profiles for other fragmentation species with m/z values equal to 12 (C^+), 19 (F^+), 44 (CO_2^+), and 51 (CHF_2^+) coincide in this range.

The intermediate decomposition product is presumably erbium fluorocarbonate, which can be evidenced by a peak on the CO_2^+ ion current curve in the range $270\text{--}310^\circ\text{C}$. Another option is to suggest the

release of carbon dioxide as a reaction product of fluorine with the material of the crucible and soot, which is often formed during the decomposition of organic species. The F^+ ion current curves show that these ions are present in the reaction area up to 500°C and, in addition, these species are in all probability consumed in the formation of CF_2^+ secondary ions, which then are converted to CO_2^+ through COF^+ : the respective curves also feature a peak in the range $270\text{--}310^\circ\text{C}$.

The solid residue is 33.5% for I and 32.4% for II, and the calculated weight loss implies that decomposition yields copper(I) oxide and erbium fluoride ($3/2\text{Cu}_2\text{O} + 2\text{ErF}_3$).

In order to verify the calculations, weights of compound I were additionally decomposed in an alundum crucible and a platinum crucible at 240 and 340°C in a muffle furnace for 4 h in a dynamic argon flow. Processing of the powder patterns of the solid decomposition residues implies that copper(I) oxide is formed at an earlier stage than erbium fluoride is (Fig. S4). PXRD data verify the calculations from TG data. The weight loss of the sample decomposed in the alundum crucible was 67.1%.

It is worth mentioning that decomposition in alundum and platinum crucibles yielded different products. The solid residue after decomposition in a platinum crucible contained some metallic copper. This distinction may be explained by the lack of interaction between the compound and the crucible material. In addition, a reddish coating of erbium fluoride was observed in both cases on the walls of the quartz reactor in which decomposition was carried out. Thus, some mass transfer of the degrading compound is observed in the systems, followed by decomposition on the hotter walls of the reactor.

The thermal behaviour of difluoroacetates and monochloroacetates differs in the high temperature range. Third and fourth decomposition stages appear for compounds III and IV, as typical of chloroacetates [35]. Their dehydration and decarboxylation occur in the same way as for I and II, as described above. At the second stage at $180\text{--}310^\circ\text{C}$, peaks can be observed in a similar set of ion current curves with m/z values equal to 12 (C^+), 16 (O^+), 35 (Cl^+), and 44 (CO_2^+), with additional ones 49 (CCl^+) and 94 ($\text{CH}_2\text{ClCOOH}^+$) (Fig. 8). At still higher temperature, however, one can observe another peak of at least equal intensity in the range $310\text{--}400^\circ\text{C}$ on the same curves except for the $m/z = 49$ and 94 curves. Apparently, only partial destruction of the carboxylate ion occurs at the second stage to break C–Cl bonds, and the remaining organic species are carboxylates modified to some extent, possibly copper carbonate. The smooth course of the TG curve does not enable one to calculate accurately the weights of intermediate compounds. However, a parallel experiment on the decomposition of sample III in a muffle furnace at 400°C and PXRD analysis of the

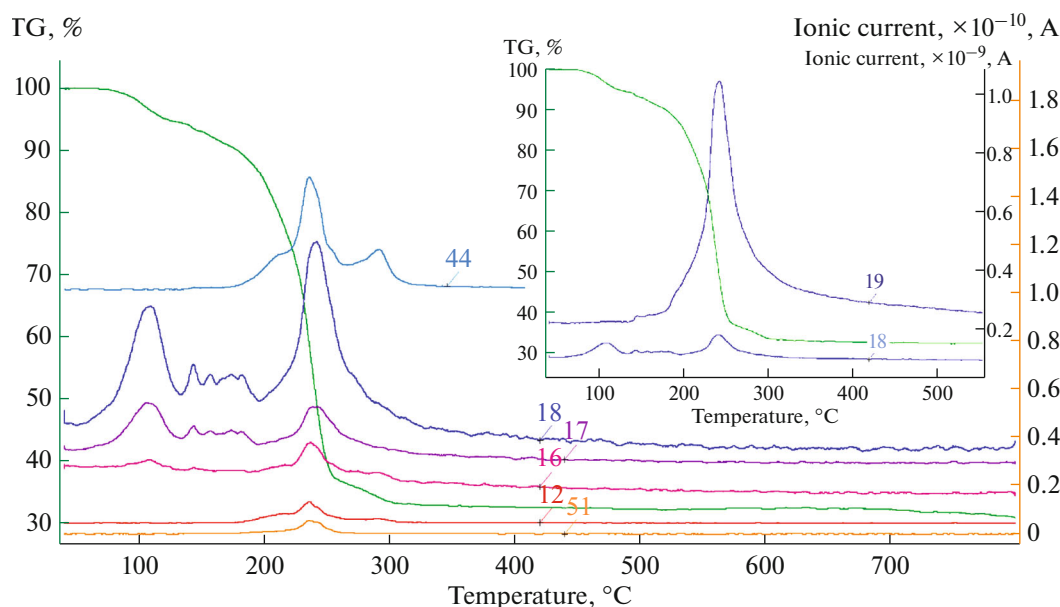


Fig. 7. TG curve for a sample of compound **I** and selected ion current curves for $m/z = 12, 16, 17, 18, 19, 44,$ and 51 .

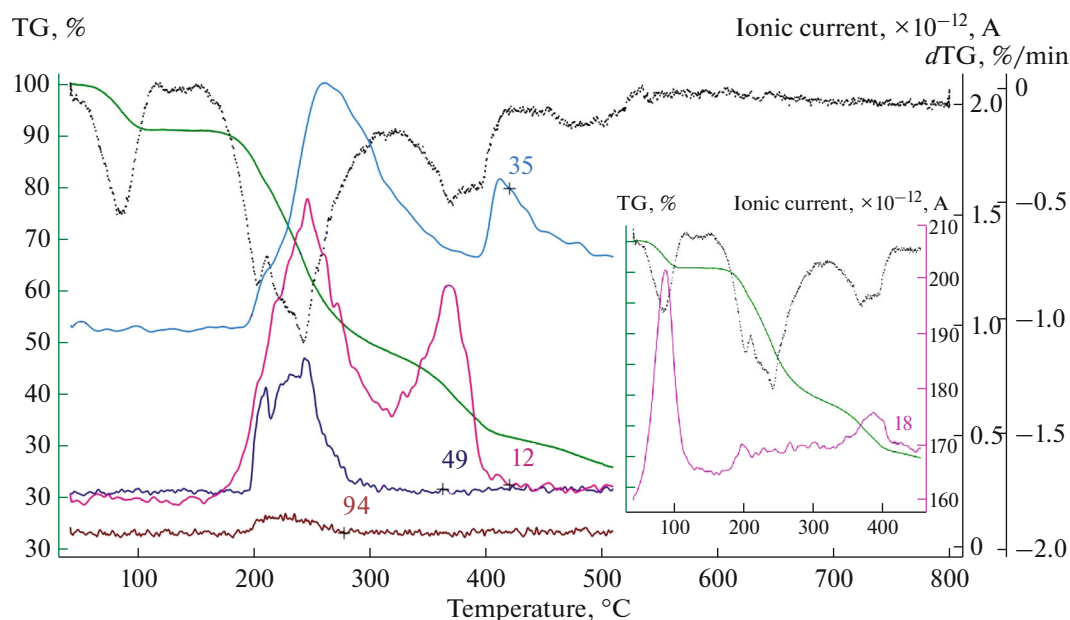


Fig. 8. TG and DTG curves for a sample of compound **III** and selected ion current curves for $m/z = 12, 18, 35, 49,$ and 94 .

solid residue showed that the major decomposition product was erbium oxochloride, a degradation product of erbium chloride hexahydrate, of which large amounts were also present in the mixture (Fig. S5). The HCl^+ and H_2O^+ ion current curves featured respective peaks at this temperature.

Zhang et al. [12] fulfilled the thermogravimetric analysis of an isostructural yttrium compound, $[\text{Cu}_3\text{Y}_2(\text{CH}_2\text{ClCOO})_{12}(\text{H}_2\text{O})_8] \cdot 2\text{H}_2\text{O}$. The authors

refer to similar decomposition temperatures, but their inferences are based exclusively on the numerical values of weight loss for ion currents for gaseous decomposition products were not recorded and X-ray powder diffraction patterns of the solid residue were not measured. Zhang et al. suppose that the second stage (210–350 °C) was complete decarboxylation to form a $\text{CuCl}_2 + 2\text{YCl}_3$ chloride mixture and the third stage (350–580 °C) was copper(II) chloride decomposition to copper(I) chloride, followed by copper(I) chloride

sublimation, and the ultimate residue in the form of erbium chloride. We cannot fully agree with their conclusions. The appearance of a broad peak of chloride ions ($m/z = 35, 37$) in the range 350–450°C can signify CuCl_2 decomposition to CuCl ; the latter, melting at 423°C, leaves the decomposition area more easily. In the solid residue at 400°C, copper is mainly CuCl and CuO , and metallic copper is only a minor impurity as probed by powder X-ray diffraction.

The TG weight loss by 530°C is 75%, which correlates with the value calculated per two erbium oxochloride units with a fraction of copper(II) oxide in the residue.

The TG data for all the four compounds are presented graphically in more details in Supplementary Information (Figs. S6–S9).

CONCLUSIONS

The cocrystallization product of individual copper and REE haloacetates are complexes that are pentanuclear molecular species. The cognated nature of the ligands (difluoro- and monochloroacetate ions) enabled isotypical compounds to be prepared, i.e., compounds having the same metal cores and unit cell parameters in spite of a qualitative difference in atomic composition.

For compound **I**, the composition and structure were determined by single-crystal X-ray diffraction, and the conditions for the formation of a single-phase crystalline sample were established. For compounds **I–IV**, the spectral characteristics were defined and their thermal stability studied. The thermal decomposition pattern of compound **I** features its reduction to monovalent copper oxide and metallic copper, as in some other carboxylates [36], and the formation of a stable REE fluoride. Chloroacetates **III** and **IV** decompose to yield the REE oxochloride, copper(II) oxide, and copper(I) chloride; CuCl is sublimed at high temperatures. The intermediate product is an REE chloride hexahydrate, which is stable over a wide range of temperatures.

Electrospray ionization mass spectrometry showed that multinuclear species formed in solution were precursors of crystalline molecular complexes.

ACKNOWLEDGMENTS

The authors are grateful to T.V. Filippova and R.A. Khalaniya for carrying out the X-ray powder diffraction studies, and to I.V. Kolesnik for recording the IR spectra. The work used equipment purchased at the expense of the Development Program of Moscow State University.

FUNDING

This work was supported by the Russian Science Foundation project No. 22-43-02020.

SUPPLEMENTARY INFORMATION

The online version contains supplementary material available at <https://doi.org/10.1134/S0036023623601678>

File ESM_1.pdf contains the following supplementary materials:

Photographic materials for compound **I** prepared by various methods (Fig. S1. Photographs of (a) single-phase crystals of compound **I** prepared as described in this paper and (b) a multiphase sample after long-term crystallization of solution with the metal molar ratio $\text{Cu} : \text{Er} = 1 : 2$);

The results of full-profile analysis (Fig. S2. Profile analysis of the X-ray diffraction pattern for a compound **II** sample.; Fig. S3. Profile analysis of the X-ray powder diffraction pattern for a compound **I** sample.);

Analysis of X-ray diffraction patterns of the decomposition products of compounds **I** and **III** (Fig. S4. Comparison of the X-ray diffraction patterns measured for solid residues of compound **I** after it was decomposed in a platinum crucible (the red line) and an alundum crucible (the blue line) at 270°C and in a platinum crucible at 240°C (the green line) with the PDF cards [S1] of erbium fluoride, copper oxide, and copper metal; Fig. S5. Comparison of the X-ray diffraction patterns measured for solid residues of compound **III** after it was decomposed in an alundum crucible at 400°C with the PDF cards [S2] of erbium chloride hexahydrate, erbium oxochloride, copper(I) chloride, copper(II) oxide, and copper metal.); and

Detailed TG data for all compounds (Fig. S6. TG results for a sample of compound **I**; Fig. S7. TG results for a sample of compound **II**; Fig. S8. TG results for a sample of compound **III**; and Fig. S9. TG results for a sample of compound **IV**).

CONFLICT OF INTEREST

The authors declare that they have no conflicts of interest.

REFERENCES

- Xu, Can, S. Chen, and L. Jia, *Russ. J. Inorg. Chem.* **67**, 22 (2022). <https://doi.org/10.1134/S0036023622601519>
- Q. Ba, J. Qian, and C. Zhang, *J. Clust. Sci.* **30**, 747 (2019). <https://doi.org/10.1007/s10876-019-01534-7>
- L. Zhong, M. Liu, and B. Zhang, et al., *Chem. Res. Chin. Univ.* **35**, 693 (2019). <https://doi.org/10.1007/s40242-019-9058-9>
- A. Vasil'ev, O. Volkova, E. Zvereva, and M. Markina, *Low Dimensional Magnetism* (FIZMATLIT, Moscow, 2018) [in Russian].
- J. B. Goodenough, *Magnetism and the Chemical Bond* (John Wiley & Sons, New Jersey, 1963).
- F. Chen, W. Lu, Y. Zhu, B. Wu, X. Zheng, *J. Coord. Chem.* **63**, 3599 (2010). <https://doi.org/10.1080/00958972.2010.514904>

7. N. Muhammad and M. Ikram, et al., *J. Mol. Struct.* **1196**, 754 (2019).
<https://doi.org/10.1016/j.molstruc.2019.06.095>
8. A. A. Bovkunova, E. S. Bazhina, I. S. Evstifeev, et al., *Dalton Trans.* **50**, 12275 (2021).
<https://doi.org/10.1039/d1dt01161h>
9. X.-M. Chen, M.-L. Tong, Y.-L. Wu, and Y.-J. Luo, *J. Chem. Soc., Dalton Trans.* **10**, 2181 (1996).
<https://doi.org/10.1039/DT9960002181>
10. V. K. Voronkova, R. T. Galeev, S. Shova, et al., *Appl. Magn. Reson.* **25**, 227 (2003).
<https://doi.org/10.1007/BF03166687>
11. Y. Cui, F. K. Zheng, D. C. Yan, et al., *Chin. J. Struct. Chem.* **17**, 5 (1998).
12. C.-G. Zhang, D. Yan, Y. Ma, and F. Yang, *J. Coord. Chem.* **51**, 261 (2000).
<https://doi.org/10.1080/00958970008055132>
13. W. Wojciechowski, J. Legendziewicz, M. Puchalska, and Z. Ciunik, *J. Alloys Compd.* **380**, 285 (2004).
<https://doi.org/10.1016/j.jallcom.2004.03.056>
14. W. G. Bateman and D. B. Conrad, *J. Am. Chem. Soc.* **37**, 2553 (1915).
15. M. D. Judd, B. A. Plunkett, and M. Pope, *J. Therm. Anal.* **9**, 83 (1976).
<https://doi.org/10.1007/BF01909269>
16. E. V. Karpova, A. I. Boltalin, Yu. M. Korenev, and S. I. Troyanov, *Russ. J. Coord. Chem.* **26**, 361 (2000).
17. G. M. Sheldrick, *Acta Crystallogr.* **A64**, 112 (2008).
<https://doi.org/10.1107/S0108767307043930>
18. G. M. Sheldrick, *Acta Crystallogr.* **A71**, 3 (2015).
<https://doi.org/10.1107/S2053273314026370>
19. G. M. Sheldrick, *Acta Crystallogr.* **C71**, 3 (2015).
<https://doi.org/10.1107/S2053229614024218>
20. K. Brandenburg and M. Berndt, *DIAMOND. Version 2.1e. Crystal Impact GbR. Bonn*, 2000.
21. J. N. Niekerk and F. R. L. Schoening, *Acta Crystallogr.* **6**, 227 (1953).
<https://doi.org/10.1107/S0365110X53000715>
22. S. Jangbo, N. Rongzhi, S. Xin, and P. Bo, *SPIE Conf. Proc.* **10256**, 1046357 (2017).
<https://doi.org/10.1117/12.2260699>
23. V. Ya. Kavun, T. A. Kaidalova, V. I. Kostin, et al., *Koord. Khim.* **10**, 1502 (1984).
24. A. S. Antsyshkina, M. A. Porai-Koshits, and V. N. Ostrikova, *Zh. Neorg. Khim.* **33**, 1950 (1988).
25. Y. Sugita and A. Ouchi, *Bull. Chem. Soc. Jpn.* **60**, 171 (1987).
<https://doi.org/10.1246/bcsj.60.171>
26. G. Oczko and P. Starynowicz, *J. Mol. Struct.* **523**, 79 (2000).
[https://doi.org/10.1016/S0022-2860\(99\)00391-9](https://doi.org/10.1016/S0022-2860(99)00391-9)
27. B. Cristovao, D. Osypiuk, B. Mirosław, and A. Bartyzel, *Polyhedron* **188**, 114703 (2020).
<https://doi.org/10.1016/j.poly.2020.114703>
28. J.-P. Costes, M. Auchel, F. Dahan, et al., *Inorg. Chem.* **45**, 1924 (2006).
<https://doi.org/10.1021/ic050587o>
29. A. N. Georgopoulou, M. Pissas, V. Psycharis, et al., *Molecules* **25**, 2280 (2020).
<https://doi.org/10.3390/molecules25102280>
30. C. G. Herbert and R. A. W. Johnstone, *Mass Spectrometry Basics* (CRC Press, New York, 2003).
<https://doi.org/10.1002/aoc.509>
31. O. Schramel, B. Michalke, and A. Kettrup, *J. Chromatogr., A* **819**, 231 (1998).
[https://doi.org/10.1016/S0021-9673\(98\)00259-3](https://doi.org/10.1016/S0021-9673(98)00259-3)
32. W. Henderson and J. S. McIndoe, *Mass Spectrometry of Inorganic, Coordination, and Organometallic Compounds* (John Wiley & Sons Ltd., New Jersey, 2005).
<https://doi.org/10.1002/0470014318>
33. G. B. Deacon and R. J. Phillips, *Coord. Chem. Rev.* **33**, 227 (1980).
[https://doi.org/10.1016/S0010-8545\(00\)80455-5](https://doi.org/10.1016/S0010-8545(00)80455-5)
34. The Matheson Company Inc., John Wiley & Sons, New Jersey, 1980.
35. O. S. Pushikhina, K. R. Volkova, E. V. Karpova, et al., *Mendeleev Commun.* **32**, 208 (2022).
<https://doi.org/10.1016/j.mencom.2022.03.018>
36. M. D. Judd, B. A. Plunkett, and M. I. Pope, *J. Therm. Anal.* **6**, 555 (1974).
<https://doi.org/10.1007/BF01911560>

Translated by O. Fedorova